Free energy minimization approach to penetration of resonant magnetic perturbations in tokamaks

D. Reiser, and M. Z. Tokar

Citation: Physics of Plasmas **16**, 122303 (2009); doi: 10.1063/1.3267845
View online: https://doi.org/10.1063/1.3267845
View Table of Contents: http://aip.scitation.org/toc/php/16/12
Published by the American Institute of Physics

Free energy minimization approach to penetration of resonant magnetic perturbations in tokamaks

D. Reiser and M. Z. Tokar
Forschungszentrum Jülich GmbH, Institute of Energy Research IEF-4: Plasma Physics, Association EURATOM-FZJ, Partner in the Trilateral Euregio Cluster, D-52425 Jülich, Germany

(Received 26 August 2009; accepted 4 November 2009; published online 3 December 2009)

By applying the principle of minimum free energy an analytical model for the plasma response to externally applied resonant magnetic perturbations (RMPs) is proposed. The results are compared with ATTEMPT code calculations [D. Reiser *et al.*, Phys. Plasmas **16**, 0042317 (2009)] and reproduce qualitatively and quantitatively the numerical results on the collisionality dependence of RMP penetration characteristics. Strong increase in the radial electric field with reduced screening at RMPs above a certain threshold is also reproduced by the model. [doi:10.1063/1.3267845]

I. INTRODUCTION

The substantial changes in plasma dynamics in tokamaks in the presence of resonant magnetic field perturbations (RMPs) have been observed in numerous experiments. Very recently it has been found that RMPs produced by special coils can be very effective in mitigation and even complete suppression of edge-localized modes.[1–4] Numerous theoretical studies have been performed in order to describe those experiments and specific features of particle and energy transport in the presence of RMPs.[5–14] Diverse mechanisms of the RMP effect on transport processes revealed in these studies rely significantly on the level of the perturbation amplitude in the edge plasma. Thus, in many investigations[13–17] the vacuum approximation considering the total magnetic field in the plasma region as a sum of the axisymmetric confinement field and the vacuum field induced by the external coils has been applied. This approximation neglects, however, a possible screening of the RMP field and the related change in the magnetic field topology. The latter is a result of a complex nonlinear interrelation of RMP field strength, plasma currents, and, in particular, plasma rotation.[18–22] In the recent numerical studies with the ATTEMPT code[23] it has been demonstrated that there is a bifurcationlike behavior of the screening of the RMP due to the electron dynamics governed by the interplay of the radial electric field and pressure gradient. These investigations were based on the solution of four-field drift-fluid equations, corresponding to the particle balance, quasineutrality condition, Ohm's law, and parallel ion momentum balance and describing the deviations of particle density n, electric potential ϕ, magnetic potential A, and parallel ion flow velocity $u_\parallel$ from equilibrium profiles,

$$\frac{\partial n}{\partial t} = -\mathbf{v}_E \cdot \boldsymbol{\nabla}(n_0 + n) + \frac{1}{e}\nabla_\parallel J_\parallel - n_0 \nabla_\parallel u_\parallel - n_0 \mathcal{K}(\phi) + \frac{T_e}{e}\mathcal{K}(n), \tag{1}$$

$$\frac{n_0 m_i}{B_0^2}\frac{\partial w}{\partial t} = -\frac{n_0 m_i}{B_0^2}\mathbf{v}_E \cdot \boldsymbol{\nabla} w + \nabla_\parallel J_\parallel + T_e \mathcal{K}(n), \tag{2}$$

$$\frac{\partial A}{\partial t} + \frac{m_e}{e^2 n_0}\frac{\partial J_\parallel}{\partial t} = -\frac{m_e}{e^2 n_0}\mathbf{v}_E \cdot \boldsymbol{\nabla} J_\parallel + \frac{T_e}{e n_0}\nabla_\parallel n - \nabla_\parallel \phi - \eta_\parallel J_\parallel, \tag{3}$$

$$n_0 m_i \frac{\partial u_\parallel}{\partial t} = -n_0 m_i \mathbf{v}_E \cdot \boldsymbol{\nabla} u_\parallel - T_e \nabla_\parallel n, \tag{4}$$

with auxiliary relations for the vorticity w and the parallel current density $J_\parallel$,

$$w = \nabla_\perp^2 \phi, \quad \mu_0 J_\parallel = -\nabla_\perp^2 A. \tag{5}$$

The curvature operator is defined by $\mathcal{K}(f) = \boldsymbol{\nabla} \cdot (\mathbf{b} \times \boldsymbol{\nabla} f / B)$, the perpendicular Laplacian by $\nabla_\perp^2 f = \boldsymbol{\nabla}^2 f - \boldsymbol{\nabla} \cdot \mathbf{bb} \cdot \boldsymbol{\nabla} f$ and the parallel derivative is given as $\nabla_\parallel f = \mathbf{b} \cdot \boldsymbol{\nabla} f$, where $\mathbf{b} = \mathbf{B}/B$ is the direction vector of the total magnetic field $\mathbf{B} = \mathbf{B}_0 + \tilde{\mathbf{B}} + \mathbf{R}$ consisting of the unperturbed equilibrium field $\mathbf{B}_0$, the internal plasma response $\tilde{\mathbf{B}} = -\mathbf{B}_0 \times \boldsymbol{\nabla} A / B_0$, and the externally induced RMP field $\mathbf{R}$. Here the parallel current density is denoted by $J_\parallel$, ϕ is the electric potential, and $\mathbf{v}_E = \mathbf{B} \times \boldsymbol{\nabla}\phi / B^2$ is the $E \times B$-velocity. The other physical parameters are the elementary charge e, the classical parallel resistivity $\eta_\parallel = m_e \nu_e / e^2 n$, with electron-collision frequency ν_e, and the electron and ion masses m_e and m_i, respectively. Cold ions are considered ($T_i = 0$) and the electron temperature T_e is assumed to be constant so the pressure p_e is controlled by the particle density n. The equilibrium state is prescribed by a particle density n_0 with a finite radial gradient $\boldsymbol{\nabla} n_0$ and $\phi = A = u_\parallel = 0$. The main results of these simulations can be summarized as follows: (i) For reactor relevant plasma parameters a RMP field can trigger a strong plasma response, with the result that induced currents establish a magnetic field structure strongly deviating from the RMP vacuum topology; (ii) the efficiency of the screening effect, produced by localized currents at the resonant surfaces and being of importance for the penetration of RMP and the width of magnetic islands, strongly depends on the plasma collisionality and the plasma beta. (iii) A threshold is observed in the dependence of the screening efficiency on the RMP field strength. Up to a certain RMP level the screening is almost complete, but for higher RMP strength the screening breaks

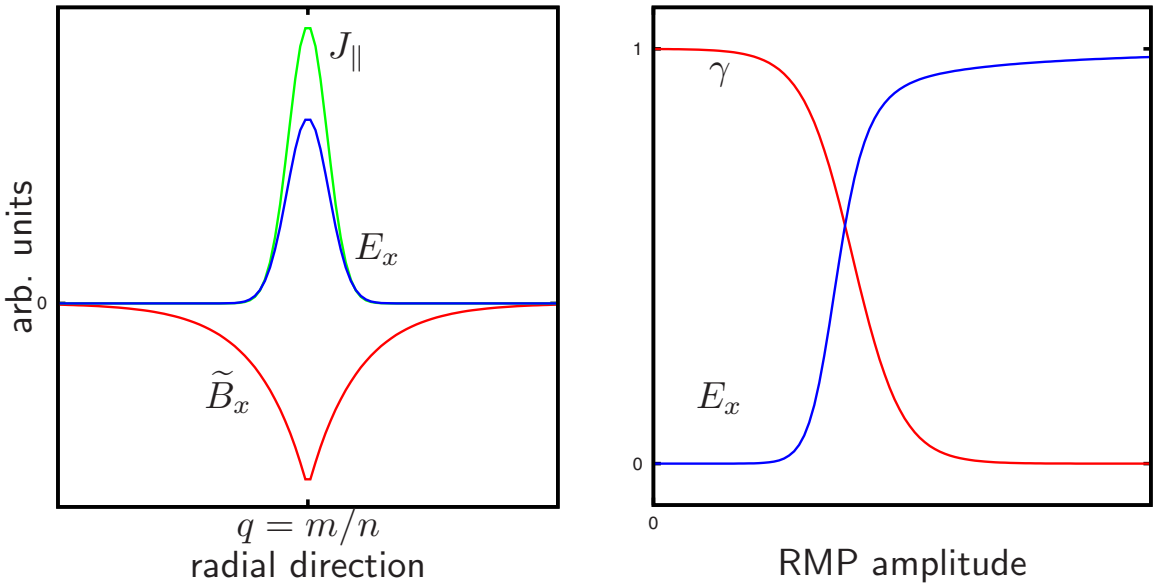

FIG. 1. (Color online) Sketch of some basic results of the screening studies of Reiser and Chandra (Ref. 23). Left: Appearance of localized shielding currents $J_\parallel$, radial magnetic fields $\widetilde{B}_x$, and radial electric fields E_x at a resonant surface with $q=m/n$. Right: Transition from strong screening efficiency γ to RMP penetration for increasing RMP amplitude and corresponding rise in the electric field and plasma rotation E_x.

down abruptly. (iv) The drop in the shielding for increasing RMP level is accompanied by an increase in the induced radial electric field and the related $E\times B$-drift flows. These findings are illustrated in Fig. 1, showing the plasma response seen as a thin layer with current $J_\parallel$ parallel to the main magnetic field and induced radial magnetic and electric field components, $\widetilde{B}_x$ and E_x, respectively. The current and the magnetic field are characterized by a dominant contribution of the resonant component with poloidal/toroidal mode numbers $m/n=q$. On the other hand, the electric field is to a large extent axisymmetric. The figure shows additionally a sketch of the variation in the screening efficiency $\gamma=-\widetilde{B}_x/R_x$ and the radial electric field with increasing RMP amplitude. Systematic numerical experiments have been performed in order to elucidate the importance of different physical mechanisms such as curvature of magnetic field, plasma viscosity, and ion parallel motion, for the behavior described above. They have shown that the new equilibrium magnetic field, i.e., the sum of the RMP field and the stationary plasma response close to the resonant surfaces, can be described quite accurately by the following reduced subset of Ohm's law and the vorticity equation (see for details Refs. 23 and 24),

$$\frac{\nabla_\parallel p_e}{en} - \nabla_\parallel \phi = \eta_\parallel J_\parallel, \tag{6}$$

$$\frac{nm_i}{B_0^2}\mathbf{v}_E\cdot\boldsymbol{\nabla}\nabla_\perp^2\phi = \nabla_\parallel J_\parallel. \tag{7}$$

In the present paper it is shown that a simple minimum free energy approach can be formulated that demonstrates that many important characteristics, e.g., RMP penetration thresholds can be estimated with an accuracy acceptable for practical purposes, by taking into account Ohm's law, Eq. (6), only. It is relevant for situations where the plasma response is dominated by the electron dynamics, as in the H-mode edge transport barrier with very sharp density gradient, unlike to the conditions where the ion dynamics, in particular, ion viscosity, is found to be crucial for bifurcationlike phenomena in the presence of RMPs. The free energy approach presented allows to get insight into the basic mechanisms of RMP penetration as they appeared in the numerical simulations and provides simple formulas to estimate the strength of the magnetic plasma response and related plasma rotation.

II. PLASMA RESPONSE AND FREE ENERGY

In order to describe the plasma response to RMP Ohm's law, Eq. (6), is considered in a periodic slab geometry with z being the coordinate along the unperturbed axisymmetric magnetic field, x the coordinate normal to the flux surface, and y denoting the binormal direction, respectively. The magnetic field is written as

$$\mathbf{B} = B_0\mathbf{e}_z + B_x\mathbf{e}_x + B_y\mathbf{e}_y \tag{8}$$

and $B_0 \gg B_x$, B_y is assumed, i.e., the deviations from the axisymmetric field are small. The components $B_x=\widetilde{B}_x+R_x$ and $B_y=\widetilde{B}_y+R_y$ contain both, the internal plasma response $\widetilde{\mathbf{B}}$ and the externally induced magnetic fields $\mathbf{R}$. This gives

$$J_\parallel = \frac{\mathbf{B}}{B}\cdot\mathbf{J} \approx J_z + \frac{B_x}{B_0}J_x + \frac{B_y}{B_0}J_y \approx J_z, \tag{9}$$

and Eq. (6) results in

$$\eta_\parallel J_z \approx \frac{B_x}{B_0}\frac{1}{en}\frac{\partial p_e}{\partial x} + \frac{B_x}{B_0}E_x + \frac{B_y}{B_0}E_y, \tag{10}$$

where E_z has been neglected. Note that here E_x denotes the deviation of the radial electric field from its value without

RMP, i.e., $E_x=0$ for $R_x=0$. The local density of the plasma free energy $\mathcal{F}$ is given as (see Ref. 25)

$$\mathcal{F}=\frac{m_i n}{2}v_E^2+\frac{m_e n}{2}\left(\frac{J_\parallel}{en}\right)^2+\frac{\tilde{B}^2}{2\mu_0}, \tag{11}$$

where the modification of the $E\times B$-velocity due to RMP is given by

$$\mathbf{v}_E=\frac{\mathbf{E}\times\mathbf{B}}{B^2}\approx\frac{E_y}{B_0}\mathbf{e}_x-\frac{E_x}{B_0}\mathbf{e}_y. \tag{12}$$

In the expression Eq. (11) for the free energy the ions contribute to the perpendicular kinetic energy and the electrons to the parallel one. At first glance one might think that the latter $\sim m_e J_\parallel^2$ is negligibly small. This is, however, not the case under consideration and this contribution is, in particular, much larger than that due to ion parallel motion. Indeed, by comparing the first and second terms on the right hand side of Eq. (3), one can find that $T_e\nabla_\parallel n\approx m_e v_E\nabla_\parallel J_\parallel/e$. By substituting this into the right hand side of Eq. (4), replacing $\nabla_\parallel\rightarrow k_\parallel$ and balancing terms, we get $m_i n_0 u_\parallel\approx m_e J_\parallel/e$, which provides the conservation of the total parallel momentum. Finally,

$$\frac{m_i n}{2}u_\parallel^2\approx\frac{m_e n}{2}\left(\frac{J_\parallel}{en}\right)^2\times\frac{m_e}{m_i}.$$

The smallness of this contribution from ion parallel motion to the free energy is also confirmed in ATTEMPT calculations. For the conditions in question, with T_e in the range of 50 eV–1 keV and $\tilde{B}$ in the order of 10^{-4} T, the last two terms in $\mathcal{F}$ are comparable if the electron parallel velocity is 1%–10% of their thermal velocity. This level can be achieved easily in strongly localized current layers arising around resonant surfaces in response to an RMP field. Here, the electron inertia can become the dominant term in the free energy. It is shown in the next sections that this forces the plasma to build up an electric field to quench the current rise. To proceed in the analysis the pressure gradient is prescribed by $\partial p_e/\partial x=-\lambda n T_e/L_\perp$ and an appropriate scaling is introduced: $v_E\rightarrow c_s v_E$, $J\rightarrow enc_s J$, $B\rightarrow\delta\sqrt{\beta}B_0 B$, and $E\rightarrow T_e E/eL_\perp$. This gives for the free energy expressed in units of $\delta^2 m_i n c_s^2/2$,

$$\mathcal{F}=E_x^2+E_y^2+(B_x-R_x)^2+(B_y-R_y)^2+\frac{1}{p^2}[B_x(E_x-\lambda)+B_y E_y]^2, \tag{13}$$

where $1/p^2=\mu\beta\delta^2/\nu^2$ represents the normalized electrical conductivity. The other dimensionless parameters are $\beta=c_s^2/v_A^2$, $\nu=\nu_e/2\omega_e$, $\delta=\rho_s/L_\perp$, $\mu=m_e/m_i$, where $c_s=\sqrt{T_e/m_i}$ and $v_A=B_0/\sqrt{\mu_0 n_0 m_i}$ are the ion sound and Alfvèn speed, respectively, $\omega_e=eB_0/m_e$ is the electron gyration frequency, and $\rho_s=m_i c_s/eB_0$ the characteristic drift scale.

In the following we seek for stable stationary states of the system corresponding to the minimum of the free energy integral $W=\int\mathcal{F}dV$ taken over the entire plasma volume, i.e., we assume that the final plasma response is determined by a minimum in the global free energy and that this minimum can be realized (see Appendix for comments on this conjecture). The field perturbations E_x, E_y, B_x, and B_y are considered as degrees of freedom and Ohm' s law, Eq. (10), as the constraint for minimization. The constraint was already taken into account in Eq. (13) when $J_\parallel$ has been expressed through the electric field and the pressure gradient. By doing this the latter was assumed unchanging in response to a RMP. This is not very realistic since numerical studies have shown that a noticeable flattening of the plasma density can happen due to increased particle transport. Nevertheless, the assumption above made for the sake of simplicity does not change the basic interplay of electric fields and pressure gradient. The results below and their comparison with results of extended numerical simulations demonstrate that despite of this approximation the simplified model is still capable to describe basic features of the RMP penetration physics qualitatively and quantitatively as well. Due to the fact that Eq. (13) does not contain any spatial derivatives of the electric and magnetic field components, the Euler–Lagrange equations to be fulfilled in this minimization problem are simply $\partial\mathcal{F}/\partial E_x=\partial\mathcal{F}/\partial E_y=\partial\mathcal{F}/\partial B_x=\partial\mathcal{F}/\partial B_y=0$. The latter are reduced to the relations

$$E_x=\frac{\lambda B_x^2}{p^2+B_x^2+B_y^2},\quad E_y=\frac{\lambda B_x B_y}{p^2+B_x^2+B_y^2}, \tag{14}$$

$$R_x=B_x\left[1+\frac{\lambda^2(p^2+B_y^2)}{(p^2+B_x^2+B_y^2)^2}\right], \tag{15}$$

$$R_y=B_y\left[1-\frac{\lambda^2 B_x^2}{(p^2+B_x^2+B_y^2)^2}\right]. \tag{16}$$

An immediate consequence of Eq. (15) is that the internal plasma response is restricted to the range $-1\leqslant\tilde{B}_x/R_x\leqslant 0$, i.e., between the limits of complete screening $\tilde{B}_x/R_x=-1$ and complete RMP penetration $\tilde{B}_x/R_x=0$. Before Eqs. (14)–(16) are analyzed in more detail in Sec. III, it is important to point out that the local minimization procedure used here is a consequence of taking into account Ohm's law as the only constraint for the global minimization problem. Therefore the local relations given by Eqs. (14)–(16) cannot be used to compute profiles of the magnetic field because the constraints due to Maxwell's equations have not been taken into account properly up to now. This point—and a remedy for practical applications—are discussed in Sec. IV. Nevertheless, the relations derived in this section contain basic features, e.g., bifurcation in screening and the rise of an electric field due to RMP fields, which survive even in the more realistic framework. Therefore, it is instructive to analyze first these implications appearing as a consequence of the Ohm's law constraint, before proceeding to the case of tokamak RMP scenarios in Sec. IV.

III. SCREENING CHARACTERISTICS

Equations (15) and (16) can be reduced to a fifth order equation for B_x. Figures 2 and 3 show examples of the variation in the screening efficiency $\gamma=1-B_x/R_x$ and radial electric field E_x with the radial perturbation field R_x.

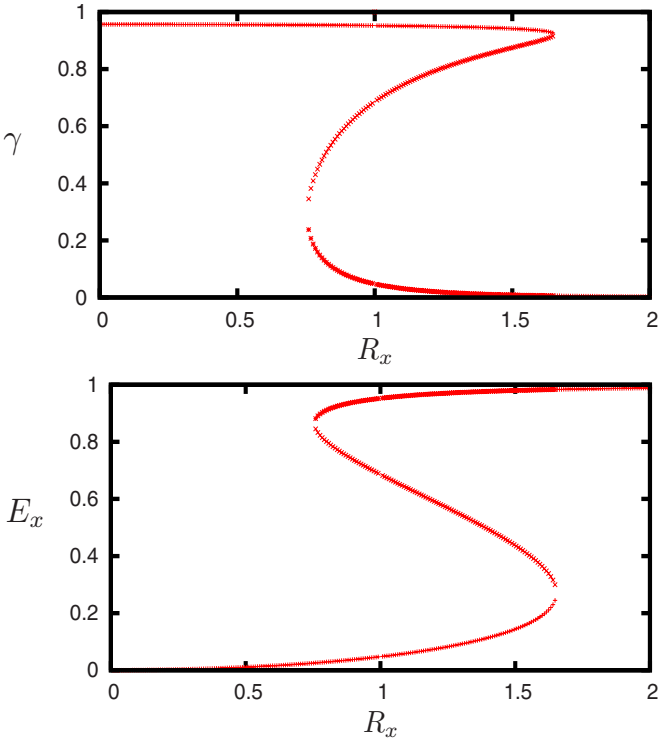

FIG. 2. (Color online) Screening efficiency $\gamma=1-B_x/R_x$ and radial electric field E_x vs radial component of the RMP magnetic perturbation R_x for $p^2=0.045$.

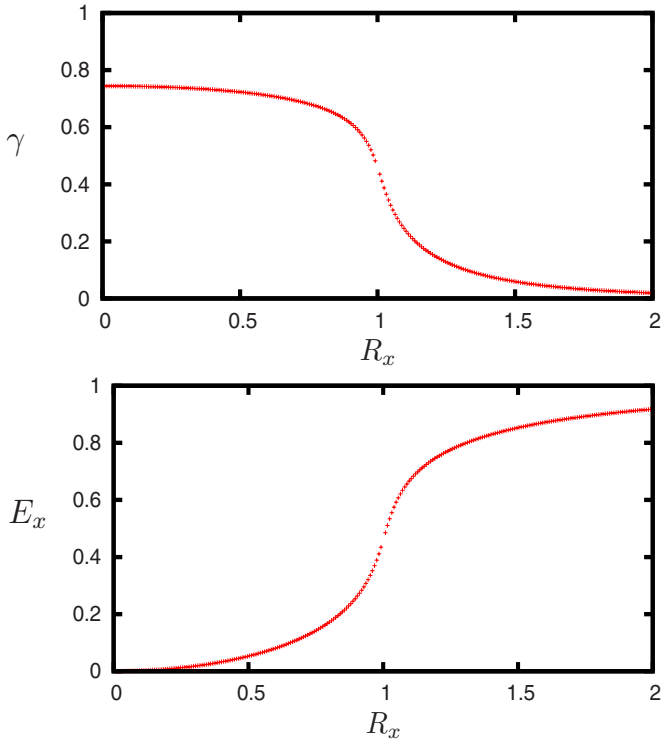

FIG. 3. (Color online) Screening efficiency $\gamma=1-B_x/R_x$ and radial electric field E_x vs radial component of the RMP magnetic perturbation R_x for $p^2=0.34$.

Computations have been done for $n=1.5\times10^{19}$ m^{-3}, $B_0=2$ T, $L_\perp=8$ cm, $\lambda=1$, and $R_y=0$ but with different plasma temperatures and thus, different resistivities p, namely, $T_e=150$ eV, $p^2=0.045$, and, $T_e=100$ eV, and $p^2=0.34$, respectively. In the case of higher electron temperature and low resistivity illustrated in Fig. 2 the screening is almost complete ($\gamma\approx1$), for low R_x, i.e., the internal plasma response nearly compensates the RMP field. For high enough RMP field $\gamma\to0$, meaning that the screening is lost and the total field is dominated by the freely penetrating RMP field. Between these two limits there is a region of ambiguity where three solutions are possible. A stability analysis proves that the solution branch in the middle is unstable, so the plasma can jump abruptly between two stable states. Due to the relation between the total magnetic field perturbation B_x and radial electric field E_x, Eq. (14), the reduction in the screening of the RMP field is inevitably connected with the rise of E_x providing a change in the plasma rotation velocity. The value $E_x=1$ corresponds to a compensation of the pressure force in Ohm's law by the electric field. The drop in the screening efficiency and the related increase in the radial electric field occur also in the case of higher resistivity, see Fig. 3. But there the transition between the regimes of high and low screening is smooth and no bifurcation is involved. In both cases the transition point is close to $R_x=1$.

In order to get some deeper insight into the bifurcation mechanism at low resistivity, Eqs. (15) and (16) are rearranged to a conditional equation for the parameter p^2 as function of B_x/R_x. According to the definition p^2 is positive, and from the analysis above it is known that $0\leqslant B_x/R_x\leqslant1$. Figure 4 shows the dependence of p^2 on the ratio B_x/R_x for different values of the perturbation field R_x. For given plasma parameters, i.e., a particular value of p^2, the possible combinations of RMP field R_x and total magnetic field B_x correspond to the intersections of the horizontal line with the curves. If the plasma collisionality is high enough and $p^2>\lambda^2/4$, i.e., $p>0.5$ for $\lambda=1$ assumed, there is only a single solution for any R_x and screening reduces smoothly with increasing RMP perturbation. For lower p three solutions become possible for R_x in some range close to $R_x=1$ with the solution in the middle being unstable. For very low R_x one finds only a single solution with strong screening and

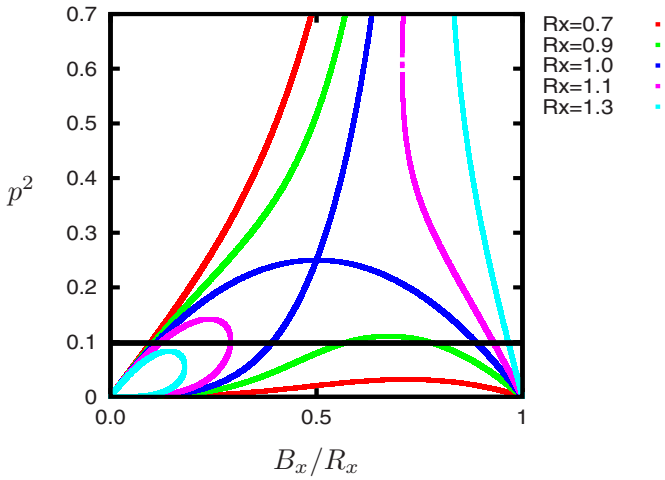

FIG. 4. (Color online) p^2 as a function of B_x/R_x for different levels of RMP perturbation. The intersections with a straight line represent the possible plasma states for a particular value of p^2.

small B_x/R_x. For very large R_x the number of possible solutions is again 1 and this corresponds to weak screening and $B_x/R_x \to 1$. With p decreasing further the range of R_x, where a bifurcation between two screening regimes is possible, becomes broader, see Figs. 2 and 3.

IV. APPLICATION TO RESONANT STRUCTURES

As mentioned at the end of Sec. II it is not reasonable to apply Eqs. (14)–(16) also to resonant structures like those appearing in tokamak RMP experiments. The free energy analysis above is a local one, and if one would consider a resonant structure and seek for the energy minimizing plasma states at each point in space by using Eqs. (14)–(16), it is not guaranteed that the three-dimensional profile of the resulting magnetic field is divergence-free and fulfills Ampére's law. In terms of calculus of variation this means that the minimization of the free energy integral $W=\int \mathcal{F} dV$ must be complemented by these constraints, e.g., via Lagrange multipliers. Taking this into account in full detail brings back all the difficulties in the solution of the general set of partial differential equations to describe the plasma dynamics. Instead of this, one could try to parametrize a meaningful model magnetic field, insert this into Eq. (13), and seek for minima with respect to the model parameters. In order to keep the analysis as simple as possible and to avoid the solution of complicated differential equations, a more simplified approach is chosen here by taking into account known properties of solutions of the extended numerical simulations performed previously. As mentioned in Sec. I the radial profile of the free energy density $\mathcal{F}$ is peaked in the vicinity of resonant surfaces and these regions are weakly overlapping for not to high magnetic shear $\hat{s}$ of order 1 and low m/n RMP fields. Therefore, the contribution of each region to W can be minimized independently. Moreover, on the basis of numerical modeling, we assume that the radial widths of these layers around the resonant surfaces, where different field perturbations are localized, are similar to each other. Thus,

$$W \sim \sum_{m,n} \langle \mathcal{F}_{m,n} \rangle \Delta_{m,n},$$

where $\mathcal{F}_{m,n}$ means $\mathcal{F}$ calculated with the field perturbations averaged over the localization regions of width $\Delta_{m,n}$, near the resonant surface with $q=m/n$ (see the sketch in Fig. 1). The bracket $\langle \cdots \rangle$ denotes a flux-surface average. In the next step the flux-surface averaged free energy density,

$$\langle \mathcal{F}_{m,n} \rangle = \langle E_x^2 \rangle + \langle E_y^2 \rangle + \langle (B_x - R_x)^2 \rangle + \langle (B_y - R_y)^2 \rangle + \frac{1}{p^2} \langle [B_x (E_x - \lambda) + B_y E_y]^2 \rangle, \tag{17}$$

is evaluated for a single mode RMP field resonant at $q=m/n$ and prescribed in the form

$$R_x = R \sin(m\vartheta - n\varphi), \quad R_y = R \cos(m\vartheta - n\varphi), \tag{18}$$

where ϑ and φ are the usual poloidal and toroidal angles, respectively. Additionally the radial electric field E_x and the total radial magnetic field B_x are split as

$$E_x = \kappa + E_x', \quad B_x = \xi \sin(m\vartheta - n\varphi) + B_x', \tag{19}$$

where $\kappa=\langle E_x \rangle$ and $\xi=2\langle B_x \sin(m\vartheta - n\varphi) \rangle$. The last separation is guided again by numerical results of extended drift-fluid simulations with the ATTEMPT code[23,24] proving that the nonprimed contributions are dominant in the respective spectra. Now the quantities κ, the flux-surface averaged radial electric field, and ξ, the resonant piece of the total magnetic field, are considered as the basic degrees of freedom of the plasma state and minimization of the free energy W is carried out with respect to these parameters. By requiring $\partial W/\partial \kappa = 0$ and $\partial W/\partial \xi = 0$, one obtains

$$\kappa = \frac{\lambda \langle B_x^2 \rangle - \langle B_x^2 E_x' + B_x B_y E_y \rangle}{p^2 + \langle B_x^2 \rangle} \tag{20}$$

and

$$\xi = \frac{p^2 R - 2\langle [(E_x - \lambda)^2 B_x' - (E_x - \lambda) B_y E_y] \sin ky \rangle}{p^2 + 2\langle (E_x - \lambda)^2 \sin^2 ky \rangle}. \tag{21}$$

According to the numerical results of three-dimensional simulations the third order contributions in the plasma response B_x, B_y, E_x, and E_y can be neglected in the expressions above, and $\kappa \gg E_x'$, $\xi \gg B_x'$. Thus, one finds approximately

$$\kappa = \frac{\lambda \xi^2}{2p^2 + \xi^2}, \quad \xi = \frac{p^2 R}{p^2 + (\kappa - \lambda)^2}. \tag{22}$$

Similar to Eqs. (15) and (16) these relations imply the restrictions $0 \leqslant \xi/R \leqslant 1$ and $0 \leqslant \kappa/\lambda \leqslant 1$ and the inspection of p^2 as a function of ξ/R—like in Fig. 4—gives bifurcation solutions for $p^2 < \lambda^2/4$, i.e., the plot of Fig. 4 can be transferred almost one-to-one just by replacing $R_x \to R/\sqrt{2}$. The resulting equation for the resonant magnetic field component ξ is

$$(\xi - R)(\xi^2 + 2p^2)^2 + 4p^2 \lambda^2 \xi = 0, \tag{23}$$

which will be used for the applications of the model in Sec. V. Note, that Eq. (23) identifies λ, the electron pressure gradient, as bifurcation parameter. For $\lambda = 0$ the bifurcation effect discussed here does not appear and $\xi = R$, i.e., complete RMP penetration, is the only possible solution. Therefore, this particular effect is not contained in previously discussed models neglecting the interplay of radial electric fields and pressure gradients in the electron momentum balance. It is also to be noted that Eqs. (22) clarify the particular role of electron inertia in our consideration of the free energy in the form of Eq. (13). For $m_e \to 0$ one finds $p^2 \to \infty$, such that $\kappa = 0$ and $\xi = R$ are the only possible solutions, i.e., again complete RMP penetration. Thus, the physical picture of the transition from screening to penetration is the following: For small RMP fields the diamagnetic character of the plasma tends to build up countercurrents to shield the externally induced RMP field. Due to the plasma resistivity the shielding currents of appropriate symmetry are localized close to resonant surfaces. At a certain level of countercurrents flowing in the plasma, it becomes more favorable to build up an electric

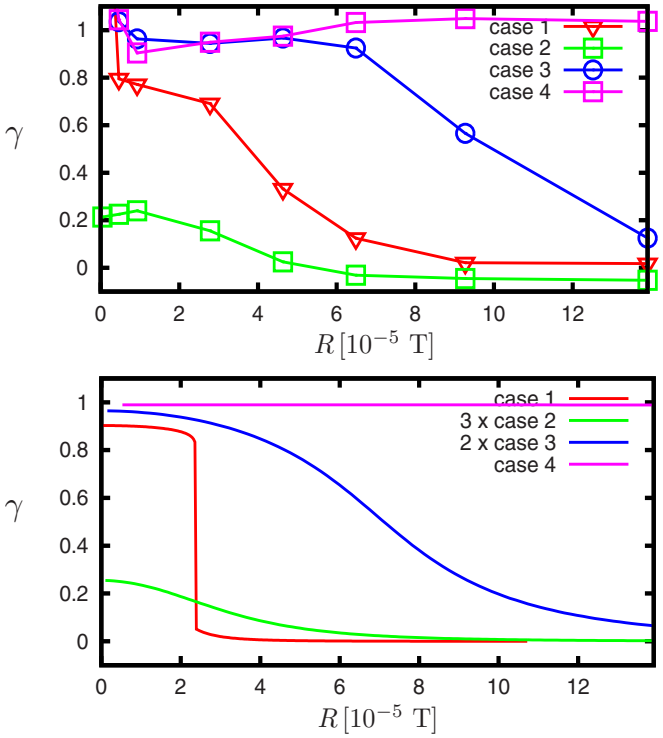

FIG. 5. (Color online) Screening efficiency for different collisionalities as a function of RMP amplitude. Case 1: $p^2=1.07\times10^{-1}$, case 2: $p^2=1.08\times10^{1}$, case 3: $p^2=1.07$, case 4: $p^2=1.06\times10^{-2}$. The results from ATTEMPT simulations are shown in the upper part and the results of the present model in the lower part.

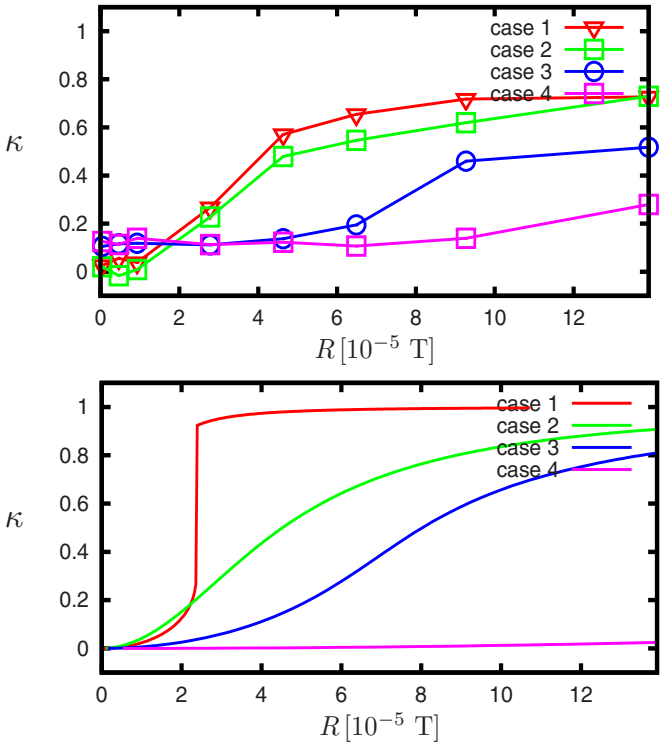

FIG. 6. (Color online) Radial electric field for different collisionalities as a function of RMP amplitude. Case 1: $p^2=1.07\times10^{-1}$, case 2: $p^2=1.08\times10^{1}$, case 3: $p^2=1.07$, case 4: $p^2=1.06\times10^{-2}$. The results from ATTEMPT simulations are shown in the upper part and the results of the present model in the lower part.

field which can—due to Ohm's law—reduce the free energy contained in the currents. The small but finite electron mass limits plasma response currents and is responsible for the bifurcation/transition discussed here.

V. COMPARISON WITH RESULTS OF 3D DRIFT-FLUID SIMULATIONS

In this section Eqs. (22) and (23) are used for a comparison with results obtained by extended three-dimensional simulations with the ATTEMPT code similar to the ones described in Ref. 23. A comparison of the screening efficiency γ and the radial electric field κ as functions of the RMP field strength R for different plasma parameters p^2 at the respective resonant surface is shown in Figs. 5 and 6. The screening efficiency obtained from three-dimensional simulations is shown in the upper part of Fig. 5. The lower part of Fig. 5 shows the results from the energy minimization model. It can be seen that the curves are in good qualitative agreement. The relative drop of the screening is reproduced quite well by the results of the simple model. However, it is found that the precise value of screening is underestimated for the cases 2 and 3 (these have been multiplied by factors of 2 and 3, respectively) and the sharp drop of case 1 is not appearing in the ATTEMPT results. On the one hand the low screening efficiencies of cases 2 and 3 can be attributed to an effective resistivity in the three-dimensional modeling which is lower than that used for the simple model. On the other hand the absence of a bifurcation is an indication that some additional effects also provide a lower bound for the resistivity. On the contrary the comparison of the results for the radial electric fields shows a remarkable agreement, even without any additional correction factors. Again the sharp variation in case 1 does not occur in the ATTEMPT results, but this is not expected due to a number of additional dissipative processes in the extended model. It is to be noted that the agreement can be improved even more, when one takes into account that the (scaled) radial electric field in the ATTEMPT simulation approaches the value of 0.7 instead of 1. This indicates that a certain density profile flattening took place and that a value of $\lambda=0.7$ would have been more appropriate for the comparison. Finally the simple model is compared with numerical results partly presented before (Figs. 3 and 4 in Ref. 23), showing the dependence of the screening efficiency on $\hat{\beta}=\hat{e}\hat{\delta}^2\beta$ and $\hat{C}=\hat{e}^2\delta\nu$, where $\hat{e}=q_0R_0/\rho_s$. Figure 7 shows a reasonable agreement of the results found by the different approaches. Again the absolute value of the screening efficiency shows a 20% discrepancy, but the qualitative behavior is reproduced quite well by the simple model.

VI. IMPLICATIONS FOR EXPERIMENTS

The examples of Sec. V have shown that the simple model presented here is well suited to provide certain characteristic quantities related to the bifurcation in the RMP penetration process. Due to the fact that this bifurcation appears at RMP levels typical for present experiments, it might be possible to check the theoretical results by comparison with experimental observations. The simple model might

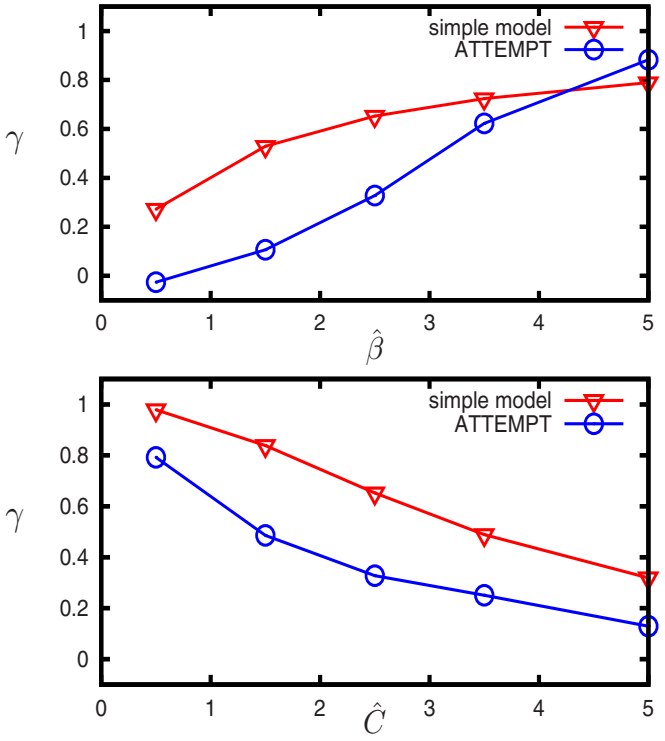

FIG. 7. (Color online) Screening efficiency as a function of $\hat{\beta}$ for fixed $\hat{C}$ (top picture) and of $\hat{C}$ for fixed $\hat{\beta}$ (bottom picture).

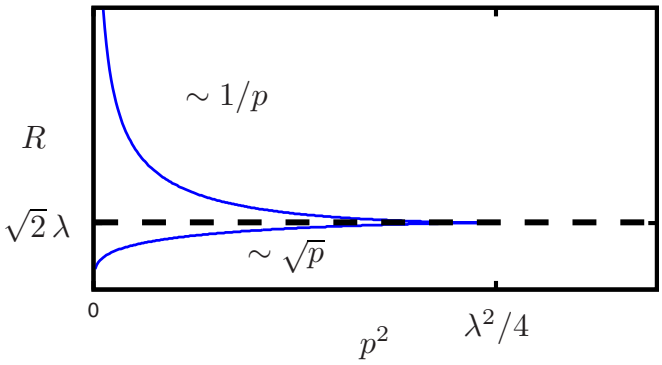

FIG. 8. (Color online) Bifurcation diagram in the R-p^2-plane. In the region between the two curves a bifurcation between states of high and low screening is possible.

also give some hints for the interpretation of experimental results, by providing quantitative limits for the bifurcation region and the validity of the vacuum approximation. Figure 8 shows the theoretically found bifurcation region in an R-p^2-plane. For p^2 below $p_c^2=\lambda^2/4$ bifurcations can take place. Solid curves show the maximum and minimum values of the RMP perturbation between which a bifurcation can appear. The upper limit obeys approximately a $1/p$-dependence and the lower one a $\sqrt{p}$-dependence. Above the bifurcation region, i.e., for quite high RMP levels, the vacuum approximation might be reasonable. For resistivities above p_c, the value $R_t=\sqrt{2}\lambda$ marks the transition point for the disappearance of RMP screening. At this point the increase in the radial electric field with the RMP level is steepest. In physical units,

$$R_t = \frac{\sqrt{2\mu_0}}{e}\frac{T_e n_0^{1/2} m_i^{1/2}}{B_0 L_\perp}, \tag{24}$$

giving, for example, $R_t=1.2\times10^{-4}$ T for $m_i=2m_p$, $B_0=2$ T, $n_0=10^{19}$ m^{-3}, $T_e=100$ eV, and $L_\perp=6$ cm. For $p^2>p_c^2$ the results show that the vacuum approximation is reasonable for $R>2R_t$. The onset of a radial electric field, described by the model presented here, might also be accessible to experimental investigations. We would like to point out again that the radial field E_x arising with increasing RMP field is the deviation from some previously existing equilibrium radial electric field. Therefore, the impact on plasma rotation can be a pure speed up, if the former equilibrium field was positive, or a braking—and perhaps a change in sign—if the former electric field was negative.

VII. SUMMARY AND CONCLUSION

The interplay of resonant magnetic field perturbations and the internal magnetic field response has been investigated on the basis of a simplified model taking into account the electron response at the resonant surfaces only. The analysis is kept on a very basic level by seeking energetically favorable plasma equilibria. On the basis of recent numerical findings[23] a simplified consideration is set up by restricting the more general model dynamics considered previously to Ohm's law along the perturbed magnetic field. The minimization of the free energy of the plasma perturbation at the resonant surfaces allows to reduce the mathematical difficulties to the solution of simple algebraic equations. The results allow to estimate the screening efficiency and change in the plasma rotation qualitatively and quantitatively. This simple model clarifies the results of sophisticated numerical computations. It is shown that in the framework of a drift-fluid model the particular screening effect observed is mainly governed by electron dynamics, whereas ion flows or ion viscosity do not play an important role. For small RMP amplitudes the plasma response is able to shield the RMP field completely and the build up of response currents is energetically more favorable than free penetration of the RMP, i.e., zero magnetic plasma response. For increasing RMP amplitude this balance is changed and a build up of an electric field limits the plasma response currents, such that the RMP field can penetrate. This transition to a rotating plasma with freely penetrating RMP field can be smooth for high plasma collisionalities, but exhibits a bifurcationlike behavior for small resistivities. The simple algebraic estimates derived here are in reasonable agreement with more sophisticated calculations and allow to quantify the transition thresholds in real plasmas to give some orientation in the interpretation of experimental scenarios, where it might be misleading to describe the magnetic field topology in the pure vacuum approximation.

APPENDIX: REMARKS ON THE FREE ENERGY MINIMIZATION

The principle of minimum plasma energy perturbation applied above is a conjecture similar to analogous concepts of minimum entropy production in nonequilibrium thermodynamics[26] or Taylor relaxation for reversed field magnetic configuration,[27] which are actually not confirmable from first principles. Nonetheless, the following arguments can be given in support of its applicability. Perturbations in magnetic and electric fields and motion of charged particles induced in the plasma as a response to the external RMP enhance the inner plasma energy. Due to radial drift motion of ions and a finite Pointing flux energy flows are generated from the volume in question which minimize the rate of the plasma energy rise. These fluxes increase the system entropy, while the increase in free energy due to ordered motion reduces entropy. Therefore, in the final steady state, where flows are reduced to zero, the perturbation of the plasma energy is minimized. Although we cannot provide a general prove of zero steady flows yet, this is indeed the case in the particular situation considered in Sec. IV, with $E_y \approx 0$ and $B_y \approx 0$. On the other hand, the free energy minimization can be regarded as a consequence of a different conjecture, where Ohm's law is turned into a minimization problem with a constraint given by the free energy in response to an externally induced RMP. In order to elucidate this we firstly rewrite the free energy minimization problem discussed in this work in the form

$$\int \mathcal{F}(E,B,J)dV = \text{minimum!},$$
$$\text{constraint: } J - G(E,B,R) = 0, \tag{A1}$$

where $\mathcal{F}$ is again the free energy density as a function of B, E, and J (denoting the magnetic field, the electric field, and the current density) and $J=G$ denotes the constraint due to Ohm's law, with R being the externally induced RMP field. The Euler–Lagrange equations for this problem are

$$\frac{\partial \mathcal{F}}{\partial B} + \frac{\partial \mathcal{F}}{\partial J}\frac{\partial \mathcal{G}}{\partial B} = 0, \tag{A2}$$

$$\frac{\partial \mathcal{F}}{\partial E} + \frac{\partial \mathcal{F}}{\partial J}\frac{\partial \mathcal{G}}{\partial E} = 0. \tag{A3}$$

This is the form derived and discussed in the previous sections. It is based on the assumption that the plasma response due to RMP fields tends to minimize the free energy. Another point of view is the following: Consider the problem

$$\int [J - G(E,B,R)]^2 dV = \text{minimum!} \equiv \epsilon,$$
$$\text{constraint: } \int \mathcal{F}(E,B,J)dV = f, \tag{A4}$$

where ϵ is a nonzero positive quantity and $f=f(R)$ depends on the RMP amplitude R only. This means that now it is assumed that Ohm's law is not fulfilled exactly and that the integral over the squared deviations from Ohm's law is never zero. However, it is also assumed that the plasma tends to minimize these deviations. This reflects quite well the physical situation (and also the numerical simulation!), where the time-averaged stationary profiles of the magnetic and electric fields considered here never perfectly fulfill Ohm's law due to the presence of fluctuations, here represented by ϵ. The (constant) integral over the free energy density serves now as a constraint for the minimization problem. The Euler–Lagrange equations for this case are

$$2(J-G)\frac{\partial G}{\partial B} + \alpha\frac{\partial \mathcal{F}}{\partial B} = 0, \tag{A5}$$

$$2(J-G)\frac{\partial G}{\partial E} + \alpha\frac{\partial \mathcal{F}}{\partial E} = 0, \tag{A6}$$

and

$$2(J-G) + \alpha\frac{\partial \mathcal{F}}{\partial J} = 0, \tag{A7}$$

where α denotes a Lagrange multiplier. Using Eq. (A7) in the relations (A5) and (A6) one finds

$$\alpha\left(\frac{\partial \mathcal{F}}{\partial B} + \frac{\partial \mathcal{F}}{\partial J}\frac{\partial \mathcal{G}}{\partial B}\right) = 0, \tag{A8}$$

$$\alpha\left(\frac{\partial \mathcal{F}}{\partial E} + \frac{\partial \mathcal{F}}{\partial J}\frac{\partial \mathcal{G}}{\partial E}\right) = 0, \tag{A9}$$

with Lagrange multiplier α determined by

$$\frac{\alpha^2}{4}\int \left(\frac{\partial \mathcal{F}}{\partial J}\right)^2 dV = \epsilon. \tag{A10}$$

Thus, for $\alpha > 0$, the Euler–Lagrange equations of the free energy minimization problem, Eqs. (A2) and (A3), and those of the "Ohm's law error minimization," Eqs. (A8) and (A9), are identical. This means that the assumed trend to fulfill the stationary Ohm's law causes a free energy minimization. Consequently, the resulting analysis is the same as presented in the previous sections. However, also this result does not give a proof for the validity of the free energy minimization approach applied in this work because the requirement of error minimization (fluctuation minimization) formulated in Eq. (A4) is a conjecture as well. Nevertheless, the different points of view discussed here—together with the reasonable agreement of results obtained from the simple model and extended simulations demonstrated in Sec. V—might support the plausibility of the approach employed.

[1] T. E. Evans, R. A. Moyer, K. H. Burrell, M. E. Fenstermacher, I. Joseph, A. W. Leonard, T. H. Osborne, G. D. Porter, M. J. Schaffer, P. B. Snyder, P. R. Thomas, J. G. Watkins, and W. P. West, Nat. Phys. **2**, 419 (2006).
[2] T. E. Evans, R. A. Moyer, P. R. Thomas, J. G. Watkins, T. H. Osborne, J. A. Boedo, E. J. Doyle, M. E. Fenstermacher, K. H. Finken, R. J. Groebner, M. Groth, J. H. Harris, R. J. La Haye, C. J. Lasnier, S. Masuzaki, N. Ohyabu, D. G. Pretty, T. L. Rhodes, H. Reimerdes, D. L. Rudakov, M. J. Schaffer, G. Wang, and L. Zeng, Phys. Rev. Lett. **92**, 235003 (2004).
[3] T. E. Evans, Nucl. Fusion **48**, 024002 (2008).
[4] M. J. Schaffer, J. E. Menard, M. P. Aldan, J. M. Bialek, T. E. Evans, and R. A. Moyer, Nucl. Fusion **48**, 024004 (2008).

[5]M. Bécoulet, G. Huysmans, P. Thomas, Ph. Ghendrih, E. Nardon, A. Grosman, X. Garbet, W. Zwingmann, R. A. Moyer, T. E. Evans, M. Schaffer, and A. Leonard, Nucl. Fusion **45**, 1284 (2005).
[6]T. E. Evans, K. H. Burrel, M. E. Fenstermacher, R. A. Moyer, T. H. Osborne, M. J. Schaffer, W. P. West, L. W. Yan, J. A. Boedo, E. J. Doyle, G. L. Jackson, I. Joseph, C. J. Lasnier, A. W. Leonard, T. L. Rhodes, P. Thomas, J. G. Watkins, and L. Zeng, Phys. Plasmas **13**, 056121 (2006).
[7]L. Yan, T. E. Evans, S. M. Kaye, and R. Maingi, Nucl. Fusion **46**, 858 (2006).
[8]E. Nardon, M. Bécoulet, G. Huysmans, O. Czarny, P. Thomas, M. Lipa, R. A. Moyer, T. E. Evans, G. Federici, Y. Gribov, A. Polevoi, G. Saibene, A. Portone, and A. Loarte, J. Nucl. Mater. **363–365**, 1071 (2007).
[9]T. E. Evans, I. Joseph, R. A. Moyer, M. E. Fenstermacher, C. J. Lasnier, and L. W. Yan, J. Nucl. Mater. **363–365**, 570 (2007).
[10]L. W. Yan and T. E. Evans, J. Nucl. Mater. **363–365**, 723 (2007).
[11]I. Joseph, T. E. Evans, A. M. Runov, M. E. Fenstermacher, M. Groth, S. V. Kasilov, C. J. Lasnier, R. A. Moyer, M. J. Schaffar, R. Schneider, and J. C. Watkins, Nucl. Fusion **48**, 045009 (2008).
[12]M. Z. Tokar, T. E. Evans, R. Singh, and B. Unterberg, Phys. Plasmas **15**, 072515 (2008).
[13]M. Z. Tokar, T. E. Evans, A. Gupta, R. Singh, P. Kaw, and R. C. Wolf, Phys. Rev. Lett. **98**, 095001 (2007).
[14]M. Z. Tokar, T. E. Evans, A. Gupta, D. Kalupin, A. Nicolai, R. Singh, and B. Unterberg, Nucl. Fusion **48**, 024006 (2008).
[15]Th. Eich, D. Reiser, and K. H. Finken, J. Nucl. Mater. **290–293**, 849 (2001).
[16]M. Kobayashi, Y. Feng, F. Sardei, D. Reiter, K. H. Finken, and D. Reiser, Nucl. Fusion **44**, S64–S73 (2004).
[17]D. Harting, D. Reiter, Y. Feng, O. Schmitz, D. Reiser, and H. Frerichs, Contrib. Plasma Phys. **48**, 99 (2008).
[18]R. Fitzpatrick and T. C. Hender, Phys. Fluids B **3**, 644 (1991).
[19]R. Fitzpatrick, Phys. Plasmas **5**, 3325 (1998).
[20]R. Fitzpatrick, Nucl. Fusion **33**, 1049 (1993).
[21]R. Fitzpatrick, Phys. Plasmas **2**, 825 (1995).
[22]A. Cole and R. Fitzpatrick, Phys. Plasmas **13**, 032503 (2006).
[23]D. Reiser and D. Chandra, Phys. Plasmas **16**, 0042317 (2009).
[24]D. Reiser, Phys. Plasmas **14**, 082314 (2007).
[25]D. Reiser and B. Scott, Phys. Plasmas **12**, 122308 (2005).
[26]G. Nicolis and I. Prigogine, *Self-Organization in Nonequilibrium Systems* (Wiley, New York, 1977).
[27]J. B. Taylor, Phys. Rev. Lett. **33**, 1139 (1974).